Theoretical and Experimental Study of Multi-Electrode Electrohydrodynamic Stimulation of Liquid Jets

A. Spohn*, P. Atten*, A. Soucemarianadin† and A. Dunand‡
****L.E.M.D., CNRS & Joseph Fourier University, Cedex, France***
†Toxot Science and Applications, Valence and Laboratoire de Rheologie, Grenoble
‡Toxot Science & Applications, Cedex, France

Introduction

As recently demonstrated[1], electrohydrodynamic (EHD) excitation of liquid jets leads to a variety of break-up modes which are inaccessible with piezoelectric stimulation. Moreover Crowley[2,3] suggested that the efficiency of EHD excitation can be increased with the help of multiple electrodes. However, little is known on the influence of the spatial distribution of the electrostatic field and the synchronization constraints imposed by the jet dynamics on such a multiple electrode exciter.

In this paper we first present a new theoretical spatio-temporal model of the behaviour of a capillary jet subjected to multielectrode stimulation. Experimental results obtained on a scaled-up prototype of an ink jet printer are found to be in good agreement with the model. In particular we examine the influence of the synchronization between the electrode spacing and the excitation wave-length. Finally the usefulness of our approach in the design of EHD drop generators is discussed.

Theoretical Model

The geometry of the axisymmetric EHD stimulation set-up is shown in Figure 1. The liquid jet of radius a leaves the nozzle with the uniform velocity U_o and passes through the four coaxial ring electrodes (ring diameter $\phi = 2b$) separated from each other by the distance Δ. Each electrode is connected with a sinusoidal high voltage power supply. Between two successive electrodes the amplitude of the voltage is inverted (phase shift of 180°). The resulting spatial and time dependent distribution of the electrostatic field imposes periodical pressure disturbances on the jet that are amplified downstream of the electrodes by the capillary instability mechanism[4]. The excitation should be optimum when there is synchronization, i.e. when the jet advances the distance Δ during the half period of the applied voltage. In this way the actions of the various electrodes add up each other and induce the highest possible jet modulation.

Since the electrostatic field has only limited axial extension the whole break-up process can be divided into two zones: A first zone where the jet is subjected to the electrostatic field and a second zone without field. Both zones can be described theoretically with the help of the long wave cylindrical jet model proposed by Lee[5] and more recently by Crowley[3]. Crowley modelled the electric field in the exciter region by a uniform spatial distribution on a given interval which does not account for its progressive evolution at the border of the electrodes. In the following, we take into account a more realistic axial distribution of the field. Indeed, to a very good approximation the field varies as $\cos(\pi x/\Delta)$ inside the electrode zone (i.e. on the interval $[0,(m\text{-}1)\Delta]$ for m electrodes). At the entrance and exit of this electrode zone the variation is different but we simplify the problem by assuming the same sinusoidal variation on an interval of length $\Delta/2$ upstream and downstream of the electrode zone.

Jet Dynamics with Electrostatic Field

Under the assumption of negligible viscous forces and in the absence of body forces the surface displacement δ, supposed to be very small, is given by the following linearized equation[3]:

$$\frac{\partial^2\delta}{\partial t^2} + 2U_o\frac{\partial^2\delta}{\partial t\partial x} + U_o^2\frac{\partial^2\delta}{\partial x^2} = -\frac{T}{2\rho a}\left[\frac{\partial^2\delta}{\partial x^2} + a^2\frac{\partial^4\delta}{\partial x^4}\right] + \frac{a}{2\rho}\frac{\partial^2 p_e}{\partial x^2} \quad (1)$$

where T is the surface tension, ρ the mass density and p_e the electrostatic pressure. In order to evaluate the importance of the different terms in (1) we introduce the following scales:

Originally published in *Proc. of IS&T's Ninth International Congress on Advances in Non-Impact Printing Technologies*, October 4-8, 1993 in Yokohama, Japan.

$$x \propto \lambda,\ t \propto 1/f,\ p_e \propto p_{eo},\ \delta \propto \delta_o, \qquad (2)$$

where $\lambda = U_o/f$ *is* the wave length of the jet deformation, f the perturbation frequency and p_{eo} the amplitude of the electrostatic pressure. If the non dimensional quantities are designed by the same symbols as in (1) we obtain:

$$\frac{\partial^2\delta}{\partial t^2} + 2\frac{\partial^2\delta}{\partial t\partial x} + \frac{\partial^2\delta}{\partial x^2} = -\frac{1}{2We}\left[\frac{\partial^2\delta}{\partial x^2} + \frac{a^2}{\lambda^2}\frac{\partial^4\delta}{\partial x^4}\right] + \frac{a}{2\delta_o}Eu_e\frac{\partial^2 p_e}{\partial x^2} \qquad (3)$$

where the Weber number $We = \rho a U_o^2 / T$ compares the dynamic pressure with the pressure caused by surface tension and the electrical Euler number $Eu_e = p_{eo} / \rho U_o^2$ compares the electrostatic pressure with the dynamic pressure. In the usual ink jet conditions:

$$We \approx O(10^2),\ Eu_e \approx O(10^{-3}). \qquad (4)$$

At the beginning of the jet evolution (inside the excitation zone), $\delta_o/a << 1$ remains small and the term with the electrostatic pressure becomes of O(l) as long as $\delta_o \approx O(10^{-3}a)$. In contrast, the influence of the surface tension can be neglected, since the Weber number is $O(10^2)$, leading to the simplified expression for (3) valid inside the stimulation zone:

$$\frac{\partial^2\delta}{\partial t^2} + 2\frac{\partial^2\delta}{\partial t\partial x} + \frac{\partial^2\delta}{\partial x^2} = \frac{a}{2\delta_o}Eu_e\frac{\partial^2 p_e}{\partial x^2} \qquad (5)$$

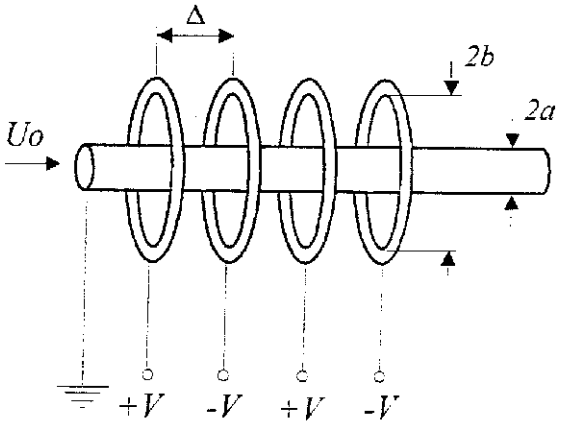

Figure 1. Schematic view of the stimulation ring electrodes around the liquid jet (note the 180° phase shift of their electrical potential).

The electrostatic pressure in (5) results from the action of the electrostatic field E on the jet surface which can be modelled by the sinusoidal distribution (non dimensional variables x and t)

$$E(x,t) = E_o \cos\pi t \cos\pi(\lambda/\Delta)x, \qquad (6)$$

in the stimulation zone $-\Delta/2 \le x \le (m - 1/2)\Delta$ and p_e is given by:

$$p_e = -(1/8)\varepsilon_o E_o^2(1+\cos 2\pi t)\,[1+\cos(2\pi(\lambda/\Delta)x)]. \qquad (7)$$

It should be noted that the frequency of the pressure variation, i.e. the frequency of the droplet generation, is 2f. Introducing (7) into (5) and defining $R = \Delta/\lambda$ gives the following linear second order equation for δ:

$$\frac{\partial^2\delta}{\partial t^2} + 2\frac{\partial^2\delta}{\partial t\partial x} + \frac{\partial^2\delta}{\partial x^2} = \frac{a\pi^2}{2\delta_o R^2}Eu_e\left[\cos\frac{2\pi x}{R} + \cos 2\pi t\cos\frac{2\pi x}{R}\right] \qquad (8)$$

The first term in the bracket on the right hand side represents a steady deformation of the jet radius in the stimulation zone. Since this term does not contribute to the time dependent radial deformation at the exit of the excitation zone, it has no effect on the perturbations that stimulate the formation of droplets and we disregard it. Setting $\delta = \mathrm{Re}[\delta_1]$, the equation governing the stimulation becomes:

$$\left(\frac{\partial}{\partial t} + \frac{\partial}{\partial x}\right)^2\delta_1 = \frac{a}{4\delta_o}\frac{\pi^2}{R^2}Eu_e\left[\exp 2\pi i(t + \frac{x}{R} + \exp 2\pi i(t - \frac{x}{R})\right] \qquad (9)$$

Introducing the following wave Ansatz

$$\delta_1 = A(x)\exp[2\pi i(t - x)], \qquad (10)$$

in (9) and integrating the obtained equation for $A(x)$ finally gives:

$$A(x_1) = \frac{aEu_e}{8\delta_0}\left[\frac{\exp(-i\pi R)}{R^2-1}\right]\left\{\frac{R^2+1}{R^2-1}[\exp(2\pi imR) - 1] - 2\pi im\right\} \qquad (11)$$

where $x_1 = [m - (1/2)]R$. The convective radial velocity

$$D\delta_1/Dt = \partial\delta_1/\partial t + \partial\delta_1/\partial x = [dA/dx]\ \exp\,[2\pi i(t - x)] \qquad (12)$$

takes at x_1 a value proportional to:

$$\left[\frac{dA}{dx}\right](x_1) = i\pi\frac{a}{4\delta_o}Eu_e\left[\frac{\exp(-i\pi R)}{(R^2-1)}\right][\exp(2\pi imR) - 1] \qquad (13)$$

Jet Dynamics without Electrical Field and Break-Up Length

Outside the stimulation zone the equation governing the surface displacement is:

$$\frac{\partial^2\delta}{\partial t^2} + 2\frac{\partial^2\delta}{\partial t\partial x} + \frac{\partial^2\delta}{\partial x^2} = -\frac{1}{2We}\left[\frac{\partial^2\delta}{\partial x^2} + \frac{a^2}{\lambda^2}\frac{\partial^4\delta}{\partial x^4}\right]. \qquad (14)$$

Following Crowley[3] and taking into account the continuity conditions for δ and $D\delta/Dt$ at the exit of the stimulation zone, the solution δ_2 of (14) can finally be written:

$$\delta_2(x,t) = [A(x_1)\cosh\mu(x-x_1) + \frac{1}{\mu}\frac{dA}{dx}(x_1)\sinh\mu(x-x_1)]\exp[2\pi i(t-x+x_1)] \quad (15)$$

where the spatial growth rate μ is defined by:

$$\mu = (2\pi/\sqrt{We})\sqrt{\left[1-(2\pi a/\lambda)^2\right]/2} \quad (16)$$

As already shown by Crowley[3], the oscillations of the radius consist of two components with amplitudes proportional to δ_1 and $(1/\mu)D\delta_1/Dt$ respectively. The second component is generally dominating since their ratio is proportional to:

$$\mu\delta_1/(D\delta_1/Dt) - |\mu/2\pi| \sim 1/\left(2\sqrt{We}\right) \quad (17)$$

which is of $O(10^{-2})$. The solution can then be approximated by neglecting the first component in (15). For large x values, the perturbation amplitude becomes, in dimensional variables:

$$\max_t|\delta_2(x,t)| = a\frac{\pi}{4\mu}Eu_e\frac{\sin(\pi mR)}{R^2-1}\exp\left(\mu\frac{x-x_1}{\lambda}\right) \quad (18)$$

The break-up length L_b can be estimated by prescribing, as usual, that the perturbation amplitude is equal to the cylindrical jet radius a. This gives:

$$\frac{L_b}{2a} = \frac{\lambda}{2a\mu}\ln\left[\frac{4\mu}{\pi Eu_e}\frac{R^2-1}{\sin(\pi mR)}\right] \quad (19)$$

We recover the logarithmic dependence of the break-up length on the amplitude of the stimulating electric field ($Eu_e \propto E_o^2$) observed with a single working electrode[3]. When $R \to 1$, the argument in the logarithm tends to a finite value and (19) becomes:

$$L_b/(2a) = (\lambda/(2a\mu))\ln[8\mu/(m\pi^2 Eu_e)] \quad (20)$$

Relation (20) shows that L_b decreases as $\ln(m)$ when there is synchronization. This indicates that the higher the number of electrodes, the smaller will be the gain obtained by adding one more electrode.

From (l9) we can see what happens when the frequency is varied. Let f_s be the frequency of synchronization. By changing f, the ratio $R = \Delta/\lambda = f/f_s$ changes and the stimulation becomes less efficient. The worst efficiency corresponds to zero values of $\sin(\pi mR)$ and, therefore, to R values equal to:

$$1/m,\ 2/m,\ \ldots,\ 1 - 1/m,\ 1 + 1/m,\ 1+2/m,\ \ldots \quad (21)$$

the set being truncated at a value such that the non dimensional wave number becomes greater than 1. From (21) we expect the working frequency interval around f_s (defined by the requirement that L_b keeps constant within a few percent) to vary as $1/m$.

Experimental Results

Experimental Arrangement

The jet of 0.4 mm in diameter is generated at the exit of a 12 mm long hypodermic needle of inner diameter ϕ = 0.45 mm. The first stimulation set-up consisted of four ring electrodes of diameter ϕ = 2.2 mm, coaxial with the jet axis (Figure 1) and located at a distance of about 1.1 mm from the nozzle. The electrodes are separated from each other by the distance Δ = 1.8 mm. Each electrode is connected to one of the two transformers that supply two sinusoidal high voltages with opposite phase. The peak amplitudes can reach up to 3 kV, while the frequency varies between 500 and 2000 Hz. Other electrode geometries (see Figure 4) are also studied which all retain the same spacing Δ = 1.8 mm.

The jet break-up is studied using the shadowgraph technique. A light emitting diode triggered by the voltage supply of the electrodes produces a shadow profile of the jet. By means of a CCD video camera this profile is displayed on a television screen together with a fixed scale located close to the jet. This allows to measure firstly the perturbation wave length λ in order to determine and control the mean velocity U_o of the jet and, secondly, the break-up length L_b. In order to obtain L_b with an accuracy better than one wave length, we used a variable phase shift between the voltage signal and the light impulse.

The working fluid is a glycerine-water mixture (65% glycerine) with viscosity η = 17 cps and surface tension $T = 64 \cdot 10^{-3}$ N/m. By adding 0.003 mol/l of tetrabutylammonium bromide the conductivity σ of the mixture is increased to 10^{-5} S/cm. In order to allow significant comparisons between different experiments, only Eu_e and R are varied during the experiments. The jet velocity is kept constant at 6.3 m/s corresponding to We = 127 and a Reynolds number Re = 85 at room temperature.

Break-up Length with Ring Electrodes

Although the last stages of the perturbation growth involves strongly non linear processes, the linear analysis allows to predict the variation of the break-up length with sufficient accuracy. In the general expression (19) for $L_b/d(d = 2a)$, the spatial growth rate μ is related with the non dimensional temporal growth rate γ through the relation $\mu a/\lambda = \gamma/\sqrt{We}$ given by (16) where

$$\gamma = k\sqrt{(1-k^2)/2} \quad \text{and} \quad k = 2\pi a/\lambda. \quad (22)$$

This is the expression given by Lee[5]. However, when using a viscous liquid we expect a non dimensional temporal growth rate γ depending on the excitation frequency and on the viscosity of the liquid. Figure 2 shows the variations of the break-up length with one, two, three and four electrodes for increasing Eu_e in the case $R \approx 1$ (synchronization). Independently of the number of electrodes all linear regression lines through the experimental points have a slope s = -21.4 which gives for γ:

$$\gamma = \sqrt{We}(\mu a/\lambda) = \sqrt{We}/(2|s|) \approx 0.27 \quad (23)$$

This value is equal to the maximum growth rate predicted by Weber[6] and is lower than the value ≈ 0.33 characterizing an inviscid liquid[5]. Here the Reynolds number $Re = O(100)$ is typical of ink jet printer conditions. Hence the result $\gamma = 0.27$ shows that, even for these rather high

Reynolds numbers, the viscous effects cannot be neglected in the break-up length estimation.

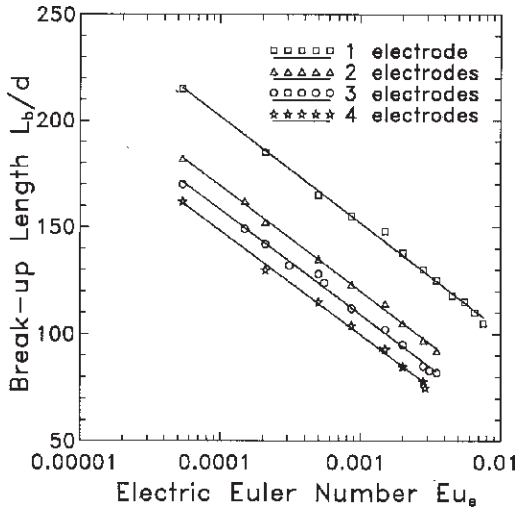

Figure 2. Break-up length with 1 to 4 ring electrodes as a function of the electric Euler Number Eu_e

From (20) it is seen that L_b should decrease like $\ln(m)$. Figure 3 shows that the observed decrease is more pronounced than predicted, but with a tendancy towards a smaller discrepancy in the slope as m increases. In particular the differences between theoretical and experimental results are most important for $m = 1$. Very likely the reason is the model of the electric field that simplifies its distribution and overestimates the electrostatic pressure in the case of one electrode or at the entrance and exit of the stimulation zone in the case of m electrodes.

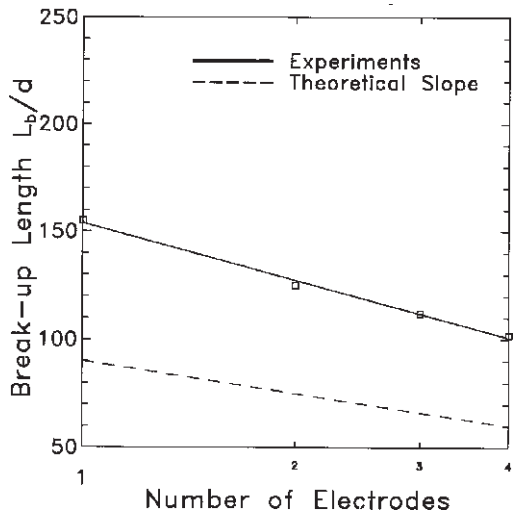

Figure 3. Break-up length as a function of the number of used ring electrodes for $Eu_e = 10^{-3}$

We can compare more directly measurements and predictions given by (20) in the case $R \approx 1$ taking for μ the value extracted from the slopes of the curves in Figure 2. The measured values of L_b are between 25 and 50 diameters longer than the predictions. Again this can be explained by the overestimation of the electrostatic pressure.

Break-Up Length for Other Electrode Geometries

The EHD stimulation is not strictly limited to electrode geometries characterized by axial symmetry. Replacing first the rings by two sets of parallel wires disposed symmetrically with respect to the jet (Figure 4a) results in only a slight increase (of about 20 d) of the break-up length. The slopes of the L_b/d curves versus $\ln(Eu_e)$ are identical and the dependence upon m is fully similar.

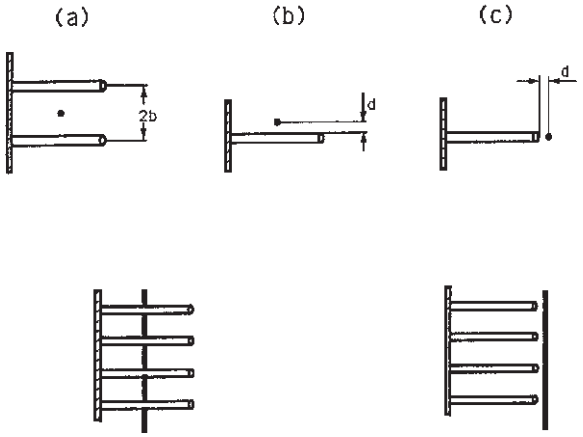

Figure 4. Asymmetrical 4 electrode geometries. Top views (upper half of the figure) and side views (lower half) of the jet/electrodes arrangement (the left side view is common to cases [a] and [b]).

Far less symmetrical geometries also lead to a satisfactory stimulation of the ink jet. A set of 4 parallel equidistant ($\Delta = 1.8$ mm) wires lying in a plane and located at a rather short distance (~ d) from the jet (Figure 4b) induce the jet break-up at downstream distances similar to those obtained with ring electrodes. Figure 5 shows that the behaviour is quite similar for both the slope ($s \cong -21.4$) and the variations with m (note that the electric Euler number is determined in a rather arbitrary way, on the basis of the coaxial ring geometry). Finally let us mention that a set of 4 needles with the tips placed close to the jet (Figure 4c), also gives the same general characteristics, the length L_b being about 25 d longer. In both cases of strong asymmetry, the A.C. field generates a permanent deviation of the jet.

Influence of the Synchronisation

Varying the frequency of the voltage applied to one electrode only results in an increase of the break-up length over the minimum value corresponding to the maximum growth rate of the perturbations. With multiple electrodes ($m \geq 2$), the effect of desynchronization can dominate over the variation of the growth rate because of the reduced efficiency of adding up effects of individual electrodes which have a relative phase shift. Such a behaviour is illustrated by Figure 6 where a 10% variation of L_b/d is obtained on the frequency intervals 1000-1800 Hz and 1170-1500 Hz for a single electrode

and a 4 electrode stimulation set-up respectively. This is in qualitative agreement with the prediction of a working frequency interval being a function of l/*m*.

Figure 6 also shows well defined maxima in the break-up length at $f_1 \cong 1000$ Hz and $f_2 \cong 1650$ Hz for $m = 4$. These maxima should correspond to the frequency values:

$$f_1 = (1-1/m)f_s = (3/4)f_s \text{ and } f_2 = (1+1/m)f_s = (5/4)f_s \quad (24)$$

The ratio $f_2/f_1 \cong 1.65$ is very close to 5/3 and the value $f_s = (f_1 + f_2)/2 \cong 1325$ Hz corresponds to the minimum break-up length. There appears a fair agreement with predictions but refined experiments are needed to obtain more detailed conclusions (existence of peaks at $f_s/4$, $f_s/2$, $2f_s$ and similar properties for other values of m).

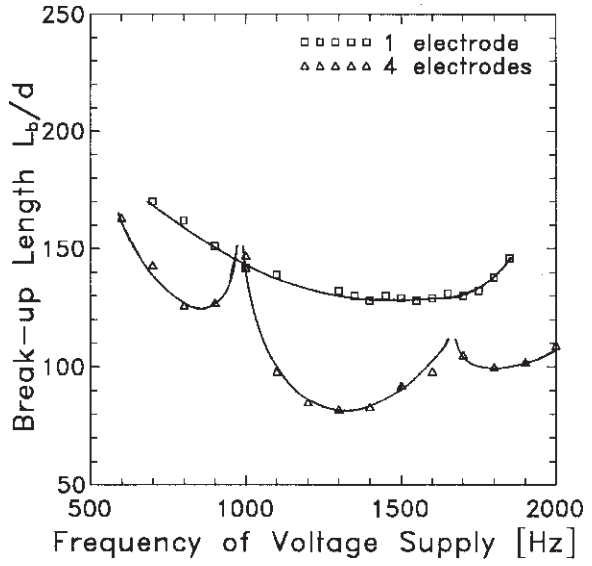

Figure 5. One set of parallel wire electrodes: Break-up length as a function of the electrical Euler number Eu_e for 1 to 4 electrodes

Conclusion

The experiments performed on a four electrode EHD exciter confirm the predictions of the model based on a simplified axial distribution of the electric field on the jet surface. The logarithmic decrease of L_b with the applied voltage is in full agreement with theory provided we retain, for the perturbation growth rate, the values given by the linear analysis taking the viscous effects into account. The observed decrease of L_b as a function of the number m of electrodes is somewhat stronger than predicted and the breakup length greater than the calculated one. This can be attributed to the employed distribution of the electric field which leads to a overestimation of the electrostatic pressure at the entrance and exit of the stimulation zone. In addition the preliminary results on the role of the frequency are in agreement with theory.

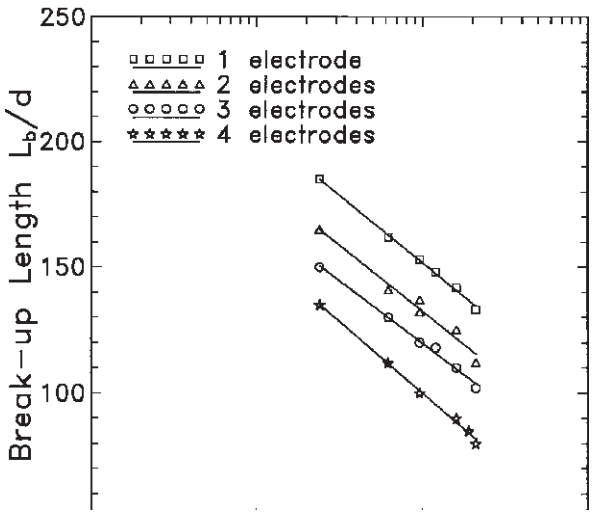

Figure 6. Break-up length as a function of the frequency of the driving voltage for 1 and 4 ring electrodes

As far as ink jet printers are concerned, the study shows that a multiple electrode exciter can be effective and can lead to reduced break-up lengths. Finally let us point out that, due to the logarithmic dependence of L_b on m and to synchronization constraints, the number of electrodes in practical devices could be rather limited.

Acknowledgements

We wish to thank the management of Toxot for permission to publish this paper and the Centre National de la Recherche Scientifique (CNRS) for partially supporting the study developed in collaboration with Toxot (contract CNRS/ IMAJE No 50.9776).

References

1. I. Rezanka and J.M. Crowley, “Satellite control by direct harmonic excitation”, *J. Imaging Techn.*, **16**, pp. 43-47, 1990.
2. J. M. Crowley, “Ink jet electrohydrodynamic excitor”, US Patent 4,220,958, 1980.
3. J. M. Crowley, “Electrohydrodynamic droplet generators”, *J. Electrostatics*, **14**, pp. 121-134, 1983.
4. Lord Rayleigh, 1896, *The theory of sound*, Vol. **II**, 2nd Edition, reprinted in 1945, Dover Publications, NewYork.
5. H. C. Lee, “Drop formation in a liquid jet”, *IBM J . Res. Develop.*, **8**, p. 364, 1974.
6. C. Weber, “Zum Zerfall eines Flüssigkeitsstrahles”, *ZAMM*, **11**, pp. 136-154, 1931.